REGULAR ARTICLE

Bone tissue engineering using 3D silk scaffolds and human dental pulp stromal cells epigenetic reprogrammed with the selective histone deacetylase inhibitor MI192

Kenny Man[1,2] · Habib Joukhdar[3] · Xue D. Manz[3,4] · Mathieu Y. Brunet[2] · Lin-Hua Jiang[5] · Jelena Rnjak-Kovacina[3] · Xuebin B. Yang[1]

Abstract

Epigenetics plays a critical role in regulating mesenchymal stem cells' (MSCs) fate for tissue repair and regeneration. There is increasing evidence that the inhibition of histone deacetylase (HDAC) isoform 3 can enhance MSC osteogenesis. This study investigated the potential of using a selective HDAC2 and 3 inhibitor, MI192, to promote human dental pulp stromal cells (hDPSCs) bone-like tissue formation in vitro and in vivo within porous *Bombyx Mori* silk scaffolds. Both 2 and 5 wt% silk scaffolds were fabricated and characterised. The 5 wt% scaffolds possess thicker internal lamellae, reduced scaffold swelling and degradation rates, whilst increased compressive modulus in comparison to the 2 wt% silk scaffold. MI192 pre-treatment of hDPSCs on 5 wt% silk scaffold significantly enhanced hDPSCs alkaline phosphatase activity (ALP). The expression of osteoblast-related genes (RUNX2, ALP, Col1a, OCN) was significantly upregulated in the MI192 pre-treated cells. Histological analysis confirmed that the MI192 pre-treated hDPSCs-silk scaffold constructs promoted bone extracellular matrix (ALP, Col1a, OCN) deposition and mineralisation compared to the untreated group. Following 6 weeks of subcutaneous implantation in nude mice, the MI192 pre-treated hDPSCs-silk scaffold constructs enhanced the vascularisation and extracellular matrix mineralisation compared to untreated control. In conclusion, these findings demonstrate the potential of using epigenetic reprogramming and silk scaffolds to promote hDPSCs bone formation efficacy, which provides evidence for clinical translation of this technology for bone augmentation.

Keywords Histone deacetylase inhibitor · Epigenetics · Silk scaffolds · Bone tissue engineering · Human dental pulp stromal cells

Introduction

The increasing ageing population and traumatic injury creates an enormous healthcare and socioeconomic burden, resulting in a major clinical need for bone tissue (Baroli 2009; Dimitriou et al. 2011; Lawlor and Yang 2019). To date, treating musculoskeletal disorders in the UK costs the National Health Service approximately £5 billion annually (Chance-Larsen et al. 2019). Current gold standard therapies to repair critical-sized bone defects, autografts suffer from limited supply and morbidity at the donor site (Berthiaume et al. 2011; Dimitriou et al. 2011). Due to these limitations, tissue engineering approaches have been explored as an alternative strategy to meet the rising demand for clinically relevant bone tissue. For bone tissue engineering, it is essential to effectively control the lineage-specific differentiation of mesenchymal stromal

✉ Xuebin B. Yang
  x.b.yang@leeds.ac.uk

1 Biomaterials & Tissue Engineering Group, School of Dentistry, University of Leeds, WTBB, St. James's University Hospital, Leeds LS97TF, UK

2 School of Chemical Engineering, University of Birmingham, Birmingham, UK

3 Graduate School of Biomedical Engineering, University of New South Wales, Sydney, Australia

4 Department of Pulmonary Medicine, Amsterdam UMC, VU University Medical Centre, Amsterdam, The Netherlands

5 School of Biomedical Sciences, University of Leeds, Leeds, UK

cells (MSCs) (Amini et al. 2012), and recent technologies such as gene therapy have garnered excitement within the field. However, these methods are associated with safety concerns such as tumourigenesis (Genetics Home Reference 2021; Maroni et al. 2012). Hence, there is a critical calling to develop novel approaches to effectively control MSCs fate for bone augmentation strategies.

Numerous studies have shown that modifying the epigenome impacts cell fate (Hu et al. 2013; Marks 2010; Maroni et al. 2012). Post-translation modifications such as acetylation have been reported to alter the cells' transcriptional activity by controlling the conformational structure of the chromatin (Tollervey and Lunyak 2012). The acetylation process is tightly regulated by two enzymes, histone acetyltransferase (HAT) and histone deacetylase (HDAC), which mediate the addition or removal of acetyl groups from lysine residues on histone proteins, respectively (Lawlor and Yang 2019). Hyperacetylation of the chromatin leads to a more open chromatin structure exhibiting increased transcriptional activity, whilst deacetylation activity results in chromatin condensation and transcriptional repression (Yang and Seto 2007). Researchers have investigated the possibility of harnessing the transcriptional plasticity of the chromatin via the use of HDAC inhibitor (HDACi) compounds, resulting in hyperacetylation (Huynh et al. 2016; Xu et al. 2007). Several studies have demonstrated the utility of modifying the epigenome with HDACis to enhance the osteogenic capacity of cells (de Boer et al. 2006; Man 2021a; Paino et al. 2014). Although promising results have been observed, the majority of studies have utilised non-selective panHDACis, which can bind to an extensive variety of HDAC isoforms, resulting in reduced differentiation efficacy and unwanted side effects (Yang et al. 2017); consequently, there is an increasing interest in using isoform-specific HDACis (Balasubramanian et al. 2009; Gryder et al. 2012). Studies have indicated that the HDAC3 isoform is causatively linked to osteogenesis due to its repression of the osteogenic transcription factor, Runx2 (Schroeder et al. 2004; Schroeder and Westendorf 2005). It has been reported that the HDAC2 and 3 selective inhibitor — MI192 is capable of enhancing the osteogenic capacity of adipose-derived MSCs (ADSCs) when compared to the use of a panHDACi Trichostatin A (TSA) (Lawlor 2016).

Moreover, the efficacy of MI192 in stimulating osteogenic differentiation and mineralisation of human dental pulp stromal cells (hDPSCs) and human bone marrow stromal cells (hBMSCs) has also been reported (Man et al. 2021b, c). Although the potential of HDACis for bone regeneration has been demonstrated, the majority of studies have evaluated their efficacy in 2D in vitro cultures, which does not replicate the conditions in situ (Abbott 2003; Baker and Chen 2012). Hence, there is a tremendous need

to investigate the therapeutic efficacy of these epigenetic modifying compounds in a more physiologically relevant microenvironment.

One of the key challenges for engineering bone tissue is using an appropriate biomaterial to provide suitable mechanical and biological properties that can mimic natural bone matrix and direct de novo tissue formation. Silk scaffolds have been utilised for multiple tissue engineering applications such as cardiac (Patra et al. 2012), neural (Allmeling et al. 2008), cartilage (Saha et al. 2013) and bone tissue engineering (Correia et al. 2012), where it has shown increasing promise. Silk is a natural biomaterial found abundantly and can be easily acquired from silkworms and spiders (Barroso et al. 2021; von Byern et al. 2019; Yoshioka et al. 2019). As well as being naturally abundant, silk possesses numerous advantageous characteristics such as being cytocompatible, easily fabricated, highly porous and biodegradability (Melke et al. 2016; Saha et al. 2013). Due to the plethora of benefits silk provides as a biomaterial, it has been utilised for numerous bone tissue engineering studies. For example, Saha et al. incorporated silk scaffolds with the osteoinductive growth factor bone morphogenetic protein 2 (Saha et al. 2013), whilst Zhao et al. applied an apatite coating to promote the osteoinductive potency of these scaffolds (Zhao et al. 2009). Meinel et al. demonstrated that silk scaffolds could repair critical-sized bone defects within mouse models (Meinel et al. 2005). As silk scaffolds have proven their potential for numerous tissue engineering applications, including bone (Correia et al. 2012; Sun et al. 2021), this biomaterial could provide a suitable platform to facilitate the delivery of MI192 pre-treated MSCs in vivo, supporting de novo bone formation.

Thus, this study aimed to explore the potential of combining MI192 pre-treated hDPSCs with porous *Bombyx Mori*-lyophilised silk scaffolds to enhance bone-like tissue formation in vitro and in vivo (Fig. 1).

Materials and methods

Silk fibroin extraction

Bombyx mori silk cocoons were purchased from Tajima Shoji Co Ltd (Japan). The silk fibroin solution was prepared (Rockwood et al. 2011) by cutting 5 g of *Bombyx mori* silk cocoons into small pieces, which was boiled in 2 L of 0.02-M sodium carbonate solution for 30 min to remove sericin. Silk fibroin fibres were washed in water and dissolved in 9.3 M lithium bromide (25% wt/v) for 4 h at 60 °C. Silk fibroin solution was dialyzed against water using SnakeSkin™ dialysis tubing (3500MWCO, Thermo Fisher Scientific) for 3 days to remove lithium bromide and centrifuged twice at 8700 RPM to remove debris. Silk fibroin
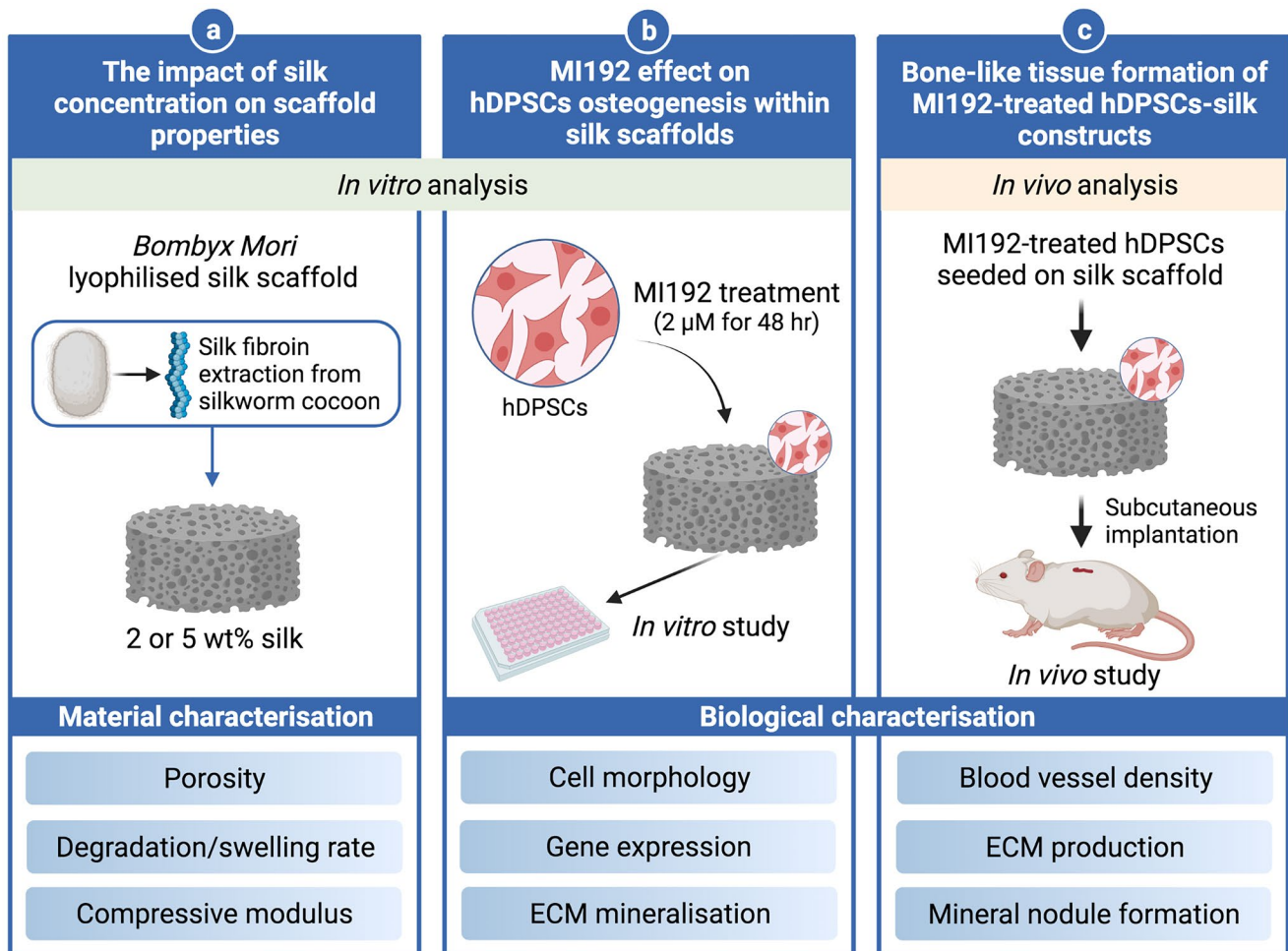
Fig. 1 Experimental outline investigating the influence of MI192 pre-treatment on osteogenic differentiation of hDPSCs within 3D silk scaffold in vitro and in vivo. **a** The influence of altering silk concentration on the scaffolds physical properties and osteogenic capacity was evaluated. **b** The effect of MI192 in stimulating hDPSCs miner-alisation within silk scaffolds in vitro was investigated. **c** Bone-like tissue formation induced by MI192 pre-treatment of hDPSCs was evaluated following 6 weeks of subcutaneous implantation in mice. (The figure was created with Biorender.com)

concentration was determined by drying a known volume of the solution and weighing the remaining film. Silk fibroin solution was stored at 4 °C. Silk fibroin is referred to as 'silk' in this article.

Silk scaffold fabrication

According to our previous research, porous silk scaffolds were fabricated by freezing a 2% or a 5% wt/v silk solution (in water) in 24-well tissue culture plates overnight at −20 °C, followed by lyophilisation and autoclaving at 121 °C to induce β-sheet formation for the formation of 2 and 5 wt% porous silk scaffolds (Rnjak-Kovacina et al. 2015). Scaffolds were hydrated in PBS and trimmed to size prior to use.

Characterisation of silk scaffolds

Dried samples were gold sputter-coated (40 mA, 60 s) and imaged with a field-emission scanning electron microscopy (SEM, Supra55VP, Zeiss, Germany) using a 5 kV electron beam. The compressive mechanical properties of the silk scaffolds were evaluated using an Instron 5543 mechanical tester with a 50 N load cell. Silk scaffolds (Ø8 mm × 4 mm) were compressed to 90% of their original height at a rate of 10 mm/min. Compressive modulus was determined between 10 and 30% strain. Silk scaffold swelling was assessed by incubating samples (Ø8 mm × 4 mm) in water or PBS and quantifying the solution uptake by mass relative to dry scaffolds. In vitro degradation was determined by incubating silk scaffolds (semicircle, Ø15 mm × 5 mm) in 2 U/ml Protease XIV solution at 37 °C for 8 days. Scaffolds were washed

in water, dried and weighed at each time point before fresh enzyme solution was added (Rnjak-Kovacina et al. 2015).

Cell isolation and in vitro expansion

HDPSCs were isolated from extracted impacted third molars obtained with patient consent through the Leeds Dental Institute/School of Dentistry, Skeletal Research Tissue Bank (REC 07/H1306/93) with ethical approval (180,615/KM/173) (El-Gendy et al. 2013). Cells were subsequently cultured in basal medium containing alpha modified minimum essential medium (α-MEM, Lonza, UK) in supplement with 10% foetal calf serum (FCS, Lonza, UK), 2-mM L-glutamine and a mix of 100 units/mL penicillin with 100 µg/ml streptomycin at 37 °C in 5% CO_2 in the air. Cells were passaged when approaching 80% confluency, and passage 4 was used for this study.

Cell seeding and osteogenic differentiation on silk scaffolds

Lyophilised silk scaffolds were cut to size (Ø5 × 2 mm) and washed with PBS. Scaffolds were then incubated in α-MEM containing 10% FCS overnight at 37 °C. Prior to adding cells, the scaffolds were washed with plain medium, and excess media within scaffolds was removed and allowed to air dry. HDPSCs were pre-treated with MI192 (2 µM for 48 h) as previously described (Man et al. 2021b). Untreated and MI192 pre-treated cells were seeded statically onto prepared scaffolds ($2 × 10^5$ cells per scaffold). Briefly, a cell suspension containing $2 × 10^5$ cells was collected by centrifugation and re-suspended in 20 µl of osteogenic medium (basal medium supplemented with 50-µM L-ascorbic acid 2-phosphate sesquimagnesium salt hydrate (Sigma-Aldrich, UK), 10-mM β-glycerol phosphate (Sigma-Aldrich, UK) and 100-nM dexamethasone (Sigma-Aldrich, UK). A cell suspension (10 µl) was placed on the bottom of a non-adherent 48 well plate (Corning, UK), and the scaffold was placed on top of the cell suspension for 10 min. After this period, the remaining cell suspension (10 µl) was transferred to the top of the scaffold, which was left to adhere for 1 h, prior to the addition of osteoinductive medium into the well. The media was changed every 3–4 days.

Cell viability and morphology on silk scaffolds 24-h post-seeding, and following 6 weeks osteoinduction was evaluated via fluorescent imaging. Briefly, media were replaced with a fresh basal medium containing CellTracker™ Green CMFDA dye and ethidium homodimer-1 (Thermo Scientific, UK) and incubated in the dark for 30 min. After incubation, scaffolds were washed in a fresh basal medium prior to imaging using a confocal laser scanning microscope (Leica, UK).

Determination of osteogenic gene expression using RT-qPCR

Cell-laden silk constructs were sliced using a sterile scalpel and placed into 500-µl RLT buffer (Qiagen, UK). Samples were vortexed and sonicated for 15 min, which was repeated four times. The lysate solution was transferred into the QIAshredder (Qiagen, UK) and centrifuged in a bench-top centrifuge at 10,000 RPM for 3 min. Cells were lysed following the RNase mini kit (Qiagen, UK) protocol. The concentration/quality of RNA was assessed using a Nanodrop spectrophotometer (Thermo Scientific, UK). RNA was converted to cDNA using a high-capacity RNA to cDNA Kit (Applied Biosystems, UK). The gene expression levels were assessed by RT-qPCR using the TaqMan gene expression assay as previously described (Man et al. 2021b). The cDNA was amplified using TaqMan primers (Supplementary Table 1) in a 20-µl reaction in a 96-well PCR plate (Starlab, UK). Amplification occurred, and the cycle threshold (C_t) was obtained within a LightCycler 480 qPCR system (Roche, UK). The comparative C_t ($2^{-\Delta\Delta Ct}$) was used for quantifying the gene expression levels (normalised by the housekeeping gene).

Alkaline phosphatase specific activity (ALPSA)

Cell-laden silk constructs were washed three times in PBS, then cut into slices using a sterile scalpel. Silk pieces were then transferred into 500 µl 0.1% Triton X-100 in PBS and were vortexed/sonicated for 5 min and then frozen at −80 °C. Samples were then thawed at 37 °C, and the lysing/freeze/thaw process was repeated four times. Following this, samples were centrifuged at $10,000 × g$ for 10 min at 4 °C, and the lysate was collected and utilised to determine ALPSA. ALP quantification was determined using the 4-nitrophenyl phosphate liquid substrate system (pNPP, Sigma-Aldrich, UK). DNA content was assessed using Pico-Green (Life Technologies, UK) as per the manufacturer's protocol. ALPSA was calculated by dividing the total ALP quantified by the total DNA content of that sample determined by PicoGreen DNA assay (nmol ALP/h/µg of DNA).

Subcutaneous implantation of cell-laden silk constructs

All procedures used were conducted under the approval of the University of Leeds Ethics Committee and under the UK Home Office project license (PPL: 70/8549). All animals in this study were 6-week-old CD1 nude male mice. A total of 5 wt% silk scaffolds were seeded with MI192 pre-treated and untreated hDPSCs as previously described. Following 24-h post-seeding, the constructs were implanted in subcutaneous pockets of each mouse

under general anaesthesia using isoflurane. At 6 weeks post-surgery, animals were euthanized, and the constructs were retrieved and fixed in 10% neutral buffered formalin (NBF, Cellpath, UK). Samples were processed for histology and immunohistochemical analysis.

Histological analysis

Fixed samples were embedded in paraffin and sectioned (4 μm) using a microtome (Leica, UK). Haematoxylin and eosin (H&E) and picrosirius red/alcian blue staining were undertaken to visualise cell distribution and collagen/glycosaminoglycans (GAGs) deposition, respectively. Calcium deposition and mineralisation were assessed via alizarin red (Millipore, UK) and Von Kossa staining (Atom Scientific, UK). Stained samples were captured under an Olympus BX50 microscope and analysed using NIS Elements BR software (Ver. 3.0). Protein deposition was assessed using an EnVision™ Detection Systems Peroxidase/DAB, Rabbit/Mouse kit (Dako, UK). Briefly, sections were placed in a PBS bath before incubation with 'Dual Endogenous Enzyme Block' from the EnVision™ kit for 10 min. Sections were washed in PBS bath for 5 min and then blocked with 20% normal goat serum (Dako, UK) in PBS for 30 min. Primary antibodies (Supplementary Table 2) were added to the samples at the desired concentration in 1% BSA (Sigma-Aldrich, UK) in PBS and left to incubate overnight at 4 °C. Sections were washed in PBS for 10 min before incubation with the secondary HRP-conjugated goat anti-rabbit IgG antibody to the samples for 30 min. After washing again in PBS for 5 min, the Dako DAB developing solution was added and incubated for 10 min prior being immersed in Harris Haematoxylin for 20 s. Samples were then examined under an Olympus BX50 microscope.

In vivo degradation was calculated from 16 H&E stained images taken from the centre of each scaffold. Degradation was semi-quantified by tracing the perimeter of internal lamellae present in the scaffold using ImageJ (National Institutes of Health, USA) (Lin et al. 2020). Similarly, mean blood vessel number was measured via ImageJ (identified through a clear lumen containing red blood cells) (16 images per sample per group).

Statistical analysis

Data expressed as mean ± standard deviation (SD). Quantitative data were statistically analysed by ANOVA multiple comparisons test with Tukey modification using SPSS software (IBM Analytics, version 21). NS: $P > 0.05$; *$P \leq 0.05$; **$P \leq 0.01$ and ***$P \leq 0.001$.

Results

Porosity and pore morphology of lyophilised silk scaffolds

SEM analysis of the 2 wt% (Fig. 2a, c) and 5 wt% (Fig. 2b, d) silk scaffolds was conducted to evaluate the porosity, pore morphology and lamellae network. The micrographs revealed a highly porous structure in both wt% groups, with a network of thin interconnected sheet-like lamellae (white arrow). The thickness of the lamellae sheets tends to increase with greater silk concentration in the scaffold.

Effects of silk concentrations on scaffold swelling, degradation and mechanical properties

Scaffold swelling in water and PBS showed a marked increase in mass following hydration of dry scaffolds (Fig. 3a). A total of 5 wt% scaffolds exhibited a significant decrease (~ 1.9 times) in the swelling capacity when compared to the 2 wt% scaffolds ($P \leq 0.001$). A total of 2 wt% silk scaffolds absorbed 32.5 ± 2.0 and 31.5 ± 1.1 times their mass in water and PBS, respectively. A total of 5 wt% scaffolds absorbed 16.9 ± 0.5 and 17.2 ± 0.4 times their mass in water and PBS, respectively.

To evaluate the effects of silk concentration on lyophilised scaffold degradation, the in vitro degradation of the scaffolds was investigated at days 2, 4, 6 or 8 after exposure to Protease XIV (Fig. 3b), showing the percent remaining mass. At each time point, the remaining mass of 2 wt% silk scaffolds was significantly lower than that of 5 wt% scaffolds ($P \leq 0.05$–0.001 respectively), demonstrating that the degradation of 2 wt% silk scaffolds was significantly faster in vitro relative to that of 5 wt% silk scaffolds.

Figure 3c, c' and d show the compressive modulus of the silk scaffolds. When compressed to 90% of their original size, 5 wt% silk scaffolds were stronger and less elastic than that of 2 wt% silk scaffolds. The compression modulus of 5 wt% scaffolds was 34.06 ± 4.52 kPa and was significantly higher (4.35 times) than that of 2 wt% silk scaffolds at 7.82 ± 0.70 kPa ($P \leq 0.001$).

Effects of silk scaffold concentration on MI192 pre-treated hDPSCs viability and osteogenic differentiation in vitro

Silk scaffolds were seeded with MI192 pre-treated or untreated hDPSCs and labelled with CFMDA to visualise the cells within the scaffolds (Fig. 4a–a'''). The

2 wt%　　　　　　　　**5 wt%**

Fig. 2 SEM micrographs showing the porosity, pore morphology and lamellae network in 2 wt% (**a**, **c**) and 5 wt% (**b**, **d**) silk scaffolds. The white arrows indicate the interconnection between the pores. The white arrowheads indicate the thin sheet-like lamellae between the pores. Scale bar, 100 μm
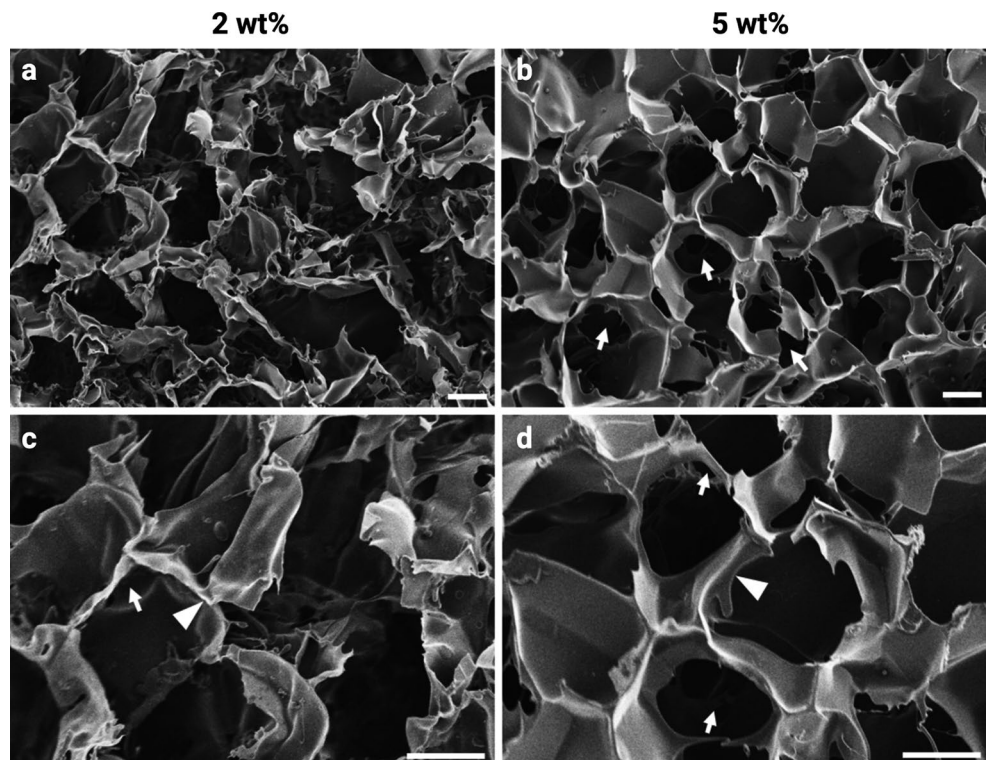
interconnectivity of the scaffolds was further confirmed by fluorescent staining, where cells were observed attached to the internal lamellae network of the scaffolds. After 24-h post-seeding, viable cells were homogeneously distributed throughout the scaffolds, with the majority of the cells possessing an elongated morphology. The MI192 pre-treated cells exhibited slightly larger/elongated morphology when compared to the untreated cells. After 6 weeks of osteogenic culture, cells in both groups were uniformly distributed throughout the scaffolds (Fig. 4b–b′′′), where cells were seen growing along with the internal lamellae pore structure. The MI192 pre-treated cells appeared to possess a slightly more elongated morphology compared to the untreated cells.

Fig. 3 Effects of silk concentration on swelling capacity (**a**), in vitro degradation (**b**) and compressive modulus (**c**, **c′**, **d**). Data expressed as mean ± SD ($n = 3$). *$P \leq 0.05$ and ***$P \leq 0.001$
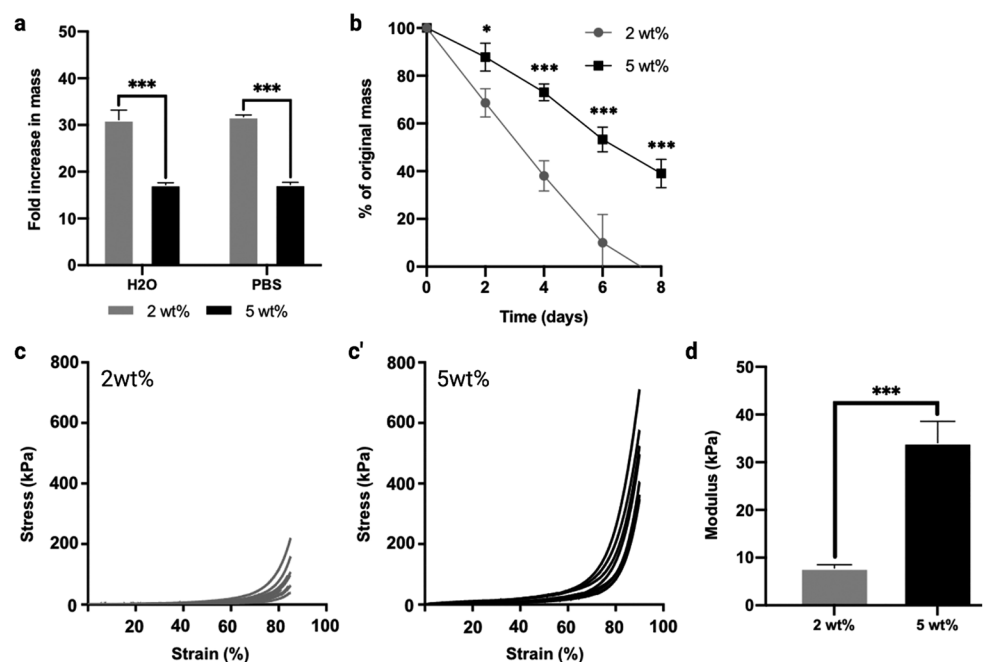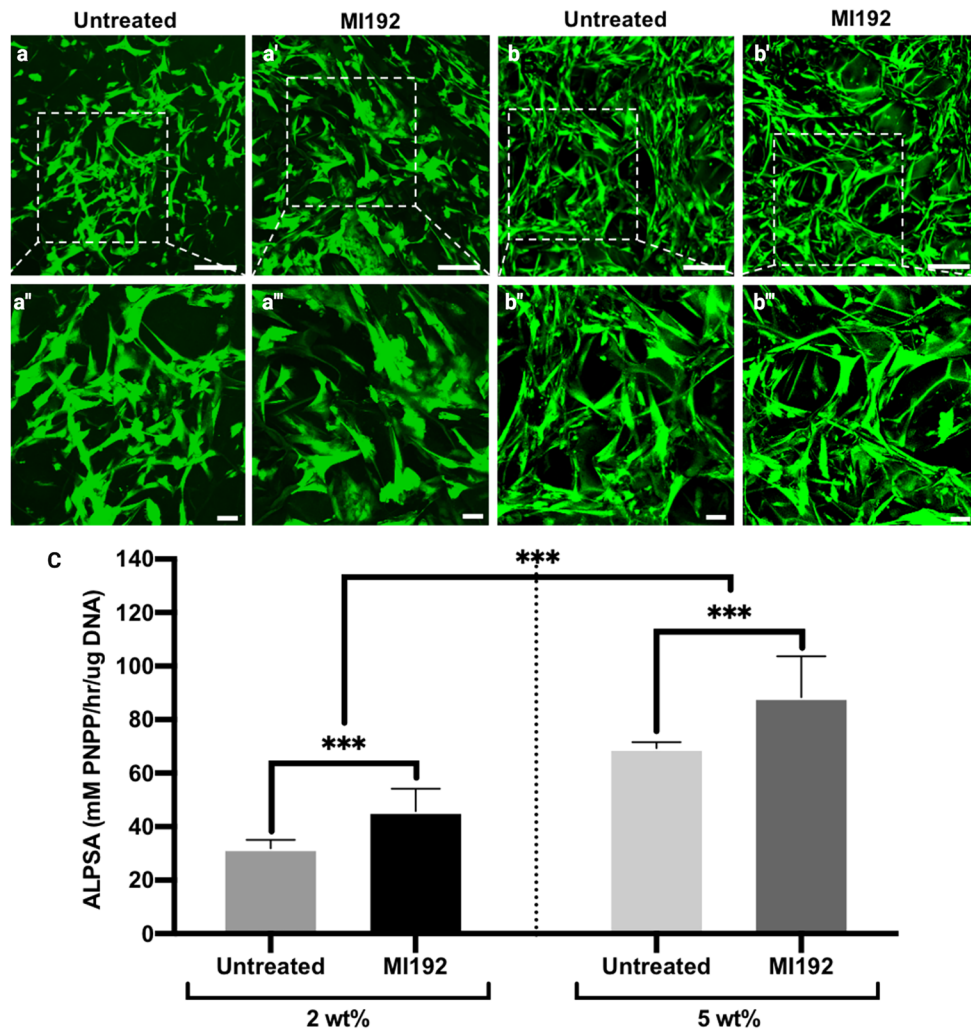
Fig. 4 The influence of silk concentrations on hDPSC viability and osteogenic capacity. Live fluorescent staining of untreated/MI192 pre-treated hDPSCs after 24 h (**a**–**a'''**) and 6 weeks (**b**–**b'''**) in osteogenic culture. Low magnification (the top panel) scale bars = 200 μm, and high magnification (the second panel) scale bars = 50 μm. **c** ALPSA of MI192 pre-treated cells on silk scaffolds following 2 weeks in osteogenic culture. Data represented as mean ± SD ($n=3$). ***$P \leq 0.001$

The influence of silk scaffold concentration on hDP-SCs osteogenic differentiation was initially assessed by quantifying ALPSA following 2 weeks of osteogenic culture (Fig. 4c). Within the 2 wt% silk scaffolds, the MI192 pre-treated cells exhibited significantly elevated ALPSA when compared to the untreated cells (2.17 times) ($P \leq 0.001$). A similar profile was observed in the 5 wt% group, where MI192 pre-treatment significantly increased ALPSA in hDPSCs (1.93 times) compared to the untreated control ($P \leq 0.001$). The MI192 pre-treated and untreated cells within the 5 wt% scaffolds elicited a significantly enhanced ALPSA compared to the cells in the 2 wt% group ($P \leq 0.001$). Therefore, the 5 wt% silk scaffolds were used for further analysis.

MI192 upregulated hDPSCs osteoblast-related gene expression within 5 wt% silk scaffolds in vitro

RT-qPCR showed the expression of the osteoblast-related genes (e.g. *RUNX2*, *ALP*, *COL1A*, *OCN*). The results showed that *RUNX2* mRNA expression was slightly reduced in the MI192 pre-treated cells compared to the untreated group on day 3 ($P > 0.05$) (Fig. 5a). After 7 days of culture, there was a significant upregulation in *RUNX2* expression in the MI192 pre-treated group compared to the untreated control ($P \leq 0.001$). However, *RUNX2* expression in the MI192 group was significantly downregulated compared to the untreated cells on day 10 ($P \leq 0.001$). *ALP* gene expression levels significantly decreased in the MI192 group when

Fig. 5 The effects of MI192 pre-treatment on the expression of osteoblast-related genes (**a-d**) in hDPSCs cultured in 5 wt% silk scaffolds during osteogenic culture. **a** *RUNX2*, **b** *ALP*, **c** *COL1A*, **d** *OCN*. Gene expression was relative to the housekeeping gene GAPDH. Data represented as mean $\pm$ SD ($n=3$). *$P \leq 0.05$, **$P \leq 0.01$ and ***$P \leq 0.001$
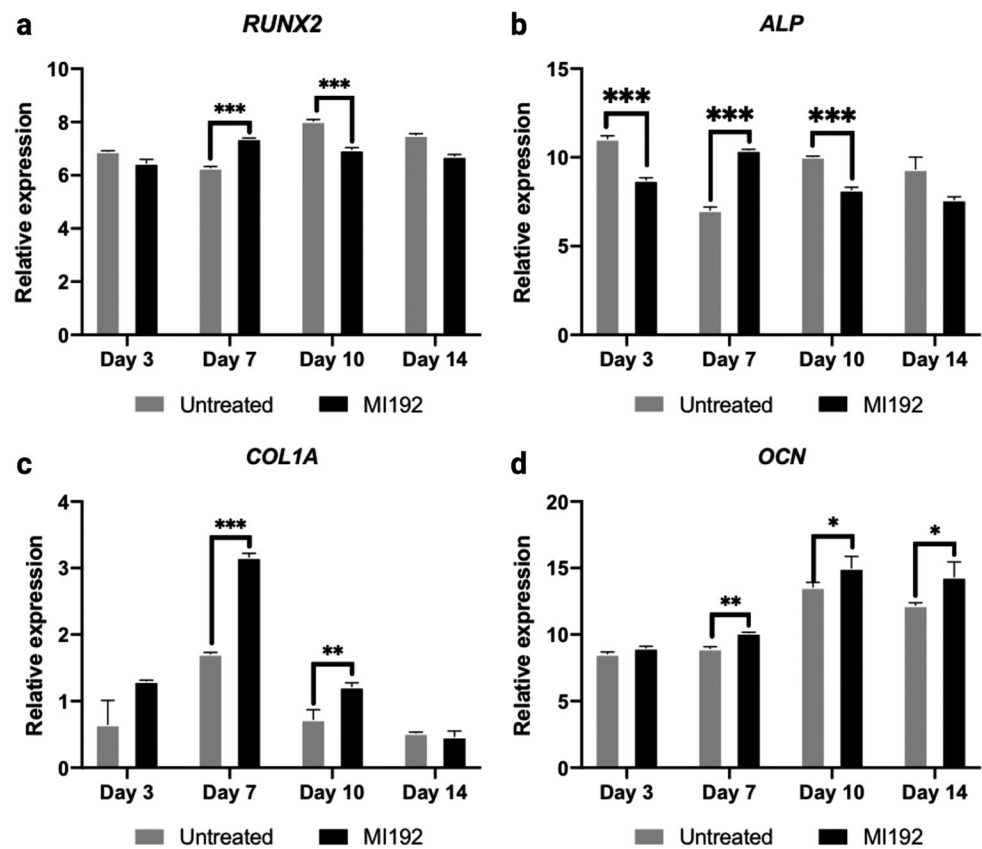
compared to the untreated cells after 3 days of osteogenic culture ($P \leq 0.001$) (Fig. 5b). On day 7, the MI192-treated cells exhibited a significant increase in *ALP* expression than the untreated control ($P \leq 0.001$). Following this, there was a significant reduction in *ALP* mRNA levels in the MI192 group on day 10 ($P \leq 0.001$). In comparison, the MI192 pre-treated cells exhibited significantly enhanced *COL1A* gene expression on both days 7 ($P \leq 0.001$) and 10 ($P \leq 0.01$) compared to the untreated cells, whilst no significance was observed on days 3 and 14 ($P > 0.05$) (Fig. 5c). The *OCN* mRNA levels were similar on day 3 ($P > 0.05$). However, the MI192-treated group displayed significantly upregulated expression of OCN compared to the untreated control on days 7, 10 and 14 ($P \leq 0.01$, $P \leq 0.05$ and $P \leq 0.05$, respectively) (Fig. 5d).

MI192 enhanced hDPSCs osteogenic protein deposition and mineralisation within 5 wt% silk scaffolds in vitro

After 6 weeks in osteogenic culture, the histological assessment showed that the samples in both groups exhibited strong picrosirius red staining for collagen deposition throughout, with the strongest intensity situated at the periphery of the scaffolds (Fig. 6a–a'''). The MI192 pre-treated group (Fig. 6a'' and a''') displayed stronger global collagen staining throughout when compared to the untreated group (Fig. 6a and a'''). Negligible staining for GAGs highlighted by alcian blue staining was observed in both constructs.

Immunohistochemical analysis showed that both MI192 pre-treated and untreated hDPSCs-silk constructs exhibited positive staining for the osteoblast-released markers assessed (ALP, Col1a and OCN), with increased protein depositions observed at the periphery of the scaffold in both groups (Fig. 6b–d). The MI192 pre-treated constructs showed substantially increased protein deposition throughout the scaffolds when compared to the untreated constructs.

The effects of MI192 pre-treatment on hDPSCs calcium deposition within the silk scaffolds were determined by alizarin red staining. The MI192 pre-treated group exhibited a significantly increased quantity of calcium deposition (1.78 fold) compared to the untreated control ($P \leq 0.001$) (Fig. 7a). The strongest accumulation of calcium deposits was situated towards the outer regions of both constructs (Fig. 7b and b'). To assess mineral nodule formation within the scaffolds, Von Kossa staining was conducted. Mineralisation was observed in both groups, particularly with increased density at the periphery of the scaffolds (Fig. 7c and c'). An enhanced quantity of black nodules
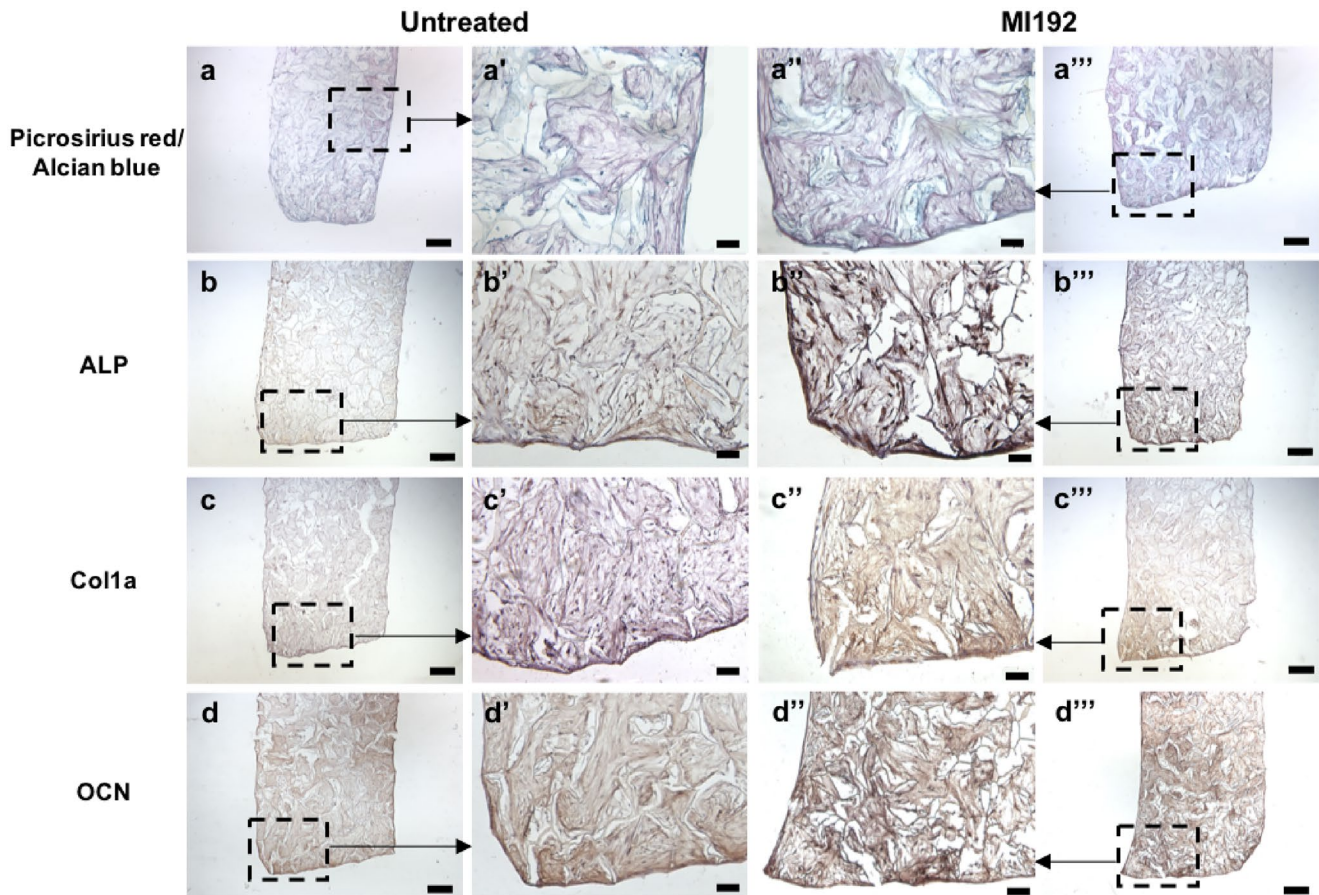
Fig. 6 Histological staining for picrosirius red and alcian blue (**a**–**a'''**) and immunohistochemical staining for ALP (**b**–**b'''**), Col1a (**c**–**c'''**) and OCN (**d**–**d'''**) of MI192 pre-treated/untreated hDPSCs on 5 wt% silk scaffolds ($n = 3$) after 6 weeks osteogenic culture in vitro. Low magnification scale bars = 200 μm (**a**–**d** and **a'''** to **d'''**), and high magnification scale bars = 50 μm (**a'** to **d'** and **a''** to **d''**)

(red arrows) were observed within the MI192 pre-treated constructs (Fig. 7c') when compared to the untreated constructs (Fig. 7c).

MI192 promoted hDPSCs extracellular bone matrix deposition and mineralisation within 5 wt% silk constructs in vivo

The subcutaneous tissue surrounding the constructs was observed through macro imaging, with evidence of vascular infiltration into the scaffolds (blue arrow) (Fig. 8a and a'). H&E staining showed that cells were distributed homogenously throughout the scaffolds, with evidence of blood vessel infiltration into the scaffolds (black arrows) in both groups (Fig. 8b and b'). Quantification of these histological images indicated a significant increase in blood vessel density within the MI192 pre-treated constructs (1.82 fold) when compared to that in the untreated constructs ($P \leq 0.01$) (Fig. 8c). There were 15.1 ± 2.1 vessels/mm^{-2} within the MI192-treated group, whilst the

untreated group exhibited 8.3 ± 1.4 vessels/mm^{-2}. There was a slight decrease in the scaffold lamellae thickness in the MI192 group when compared to that of the untreated group, although the decrease was not significant (Fig. 8d) ($P > 0.05$).

The effects of MI192 pre-treatment on hDPSCs extracellular matrix deposition and mineralisation within constructs following subcutaneous implantation was investigated via histological analysis (Fig. 9). Picrosirius red/alcian blue staining showed that both groups possessed strong staining for collagen deposition, with increased intensity observed in the MI192 group (Fig. 9a and a'). Von Kossa staining confirmed that MI192 pre-treatment enhanced nodule formation compared to the untreated constructs (Fig. 9b and b'). Immunohistochemical analysis showed the effects of MI192 on hDPSCs extracellular matrix production within silk scaffolds in vivo. Positive immunostainings for Col1a (Fig. 9c and c') and OCN (Fig. 9d and d') were observed in both MI192 pre-treated and untreated groups, with the MI192 pre-treated group exhibiting increased protein deposition compared to the untreated control.
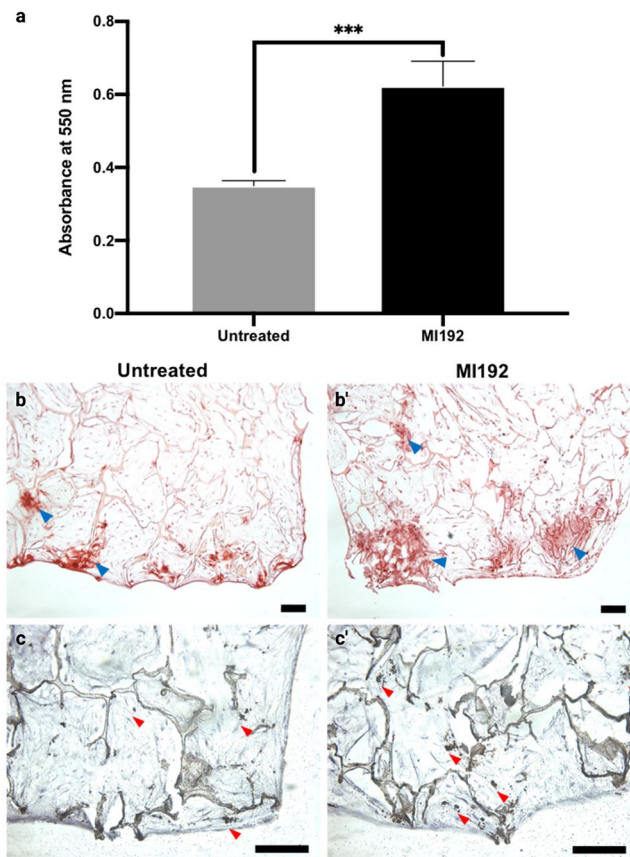
Fig. 7 Effects of MI192 pre-treatment on hDPSCs calcium accumulation and mineralisation within 5 wt% silk scaffolds after 6 weeks osteogenic culture. **a** Quantitative alizarin red analysis, **b** & **b'** alizarin red staining (red colour: blue arrowheads), **c** and **c'**) Von Kossa staining (black colour: red arrowheads). Data represented as mean ± SD ($n = 3$). ***$P \leq 0.001$. Scale bar, 100 µm

Discussion

Epigenetic modifications are known to control transcriptional activity, with HDACis demonstrating their potential for enhancing MSCs' osteogenic capacity (Cho et al. 2005; Man et al. 2021b; Paino et al. 2014). The majority of studies have focussed on assessing the efficacy of these epigenetic modifying compounds in 2D in vitro culture, with limited use of 3D in vitro models. Over the last decade, there have been an increased number of reports on the use of HDACis for bone regeneration in vivo. For example, Lee et al. (2011) utilised a collagen scaffold and a calcium phosphate scaffold soaked with Largazole for the repair of a calvarial bone defect model (Lee et al. 2011). Similarly, Jung et al. (2010) combined a calcium sulphate scaffold with TSA to stimulate osteogenic differentiation in vitro and in vivo (Jung et al. 2010). Importantly, these studies have employed non-selective panHDACis, which exhibit reduced differentiation efficacy compared to selective HDACis and are associated

with potential side effects from inhibiting a broad range of HDAC isoforms (Lawlor 2016; Yang et al. 2017). Hence, there is great precedence to shift towards the use of selective HDACis for bone augmentation strategies (Yamauchi et al. 2020). In this study, the efficacy of a selective HDAC2 and 3 inhibitor — MI192 to stimulate hDPSCs osteogenic capacity within the *Bombyx Mori* lyophilised silk scaffolds — was investigated in vitro and in vivo.

Due to silk's favourable properties for tissue engineering (Melke et al. 2016; Sun et al. 2021), it has been increasingly combined with epigenetic strategies for bone regeneration. For example, Han et al. (2015) reported hBMSCs overexpressing the H4K20/H3K9 demethylase PHF8, accelerated craniofacial and bone development when delivered within a silk fibroin scaffold in mice (Han et al. 2015). Hence, the potential use of silk scaffolds to facilitate epigenetically enhanced MSCs for bone repair has been demonstrated. In this study, we have found that the silk scaffolds displayed a highly porous surface topography, which is similar to the data reported in the literature (Saha et al. 2013; Uebersax et al. 2006; Varkey et al. 2015). Moreover, these scaffolds exhibited a thin sheet-like lamellae network, where increasing the silk concentration resulted in thicker lamellae. This is expected as more ice crystals form within the negative cast of the pores during the fabrication process, thus displacing the silk dissolved in the solution and creating a concentrated silk layer surrounding the fully formed crystal (Joukhdar et al. 2021). Hence, the increased lamellae thickness of the 5 wt% scaffold can be attributed to an increased quantity of silk available to concentrate around the ice crystals during fabrication. Mechanical characterisation showed that the 5 wt% silk scaffold was stronger and less elastic with compression modulus approximately fourfold higher than the 2 wt% scaffolds, consistent with previous findings (Rnjak-Kovacina et al. 2015).

Additionally, in vitro degradation of such silk scaffolds was a function of the silk concentration, where the 2 wt% scaffolds degraded at a much higher rate compared to the 5 wt% group following exposure to protease XIV, correlating with the findings in the literature (Rnjak-Kovacina et al. 2015). The enhanced mechanical properties exhibited by the higher percentage scaffold is beneficial for bone tissue engineering applications in not only supporting the defect site immediately post-implantation but also promoting MSCs osteogenic differentiation through increased mechanotransductive stimulation (Ghasemi-Mobarakeh et al. 2015; Sun et al. 2018). Moreover, numerous studies have reported the role of biomaterials in augmenting important epigenetic functions via the modification of the cell's actin cytoskeleton that transmits forces to the nuclear protein lamin A/C, ultimately resulting in increased transcriptional activation (Downing et al. 2013; Li et al. 2011). For example, 3D-printed titanium scaffolds exhibiting a triangle pore
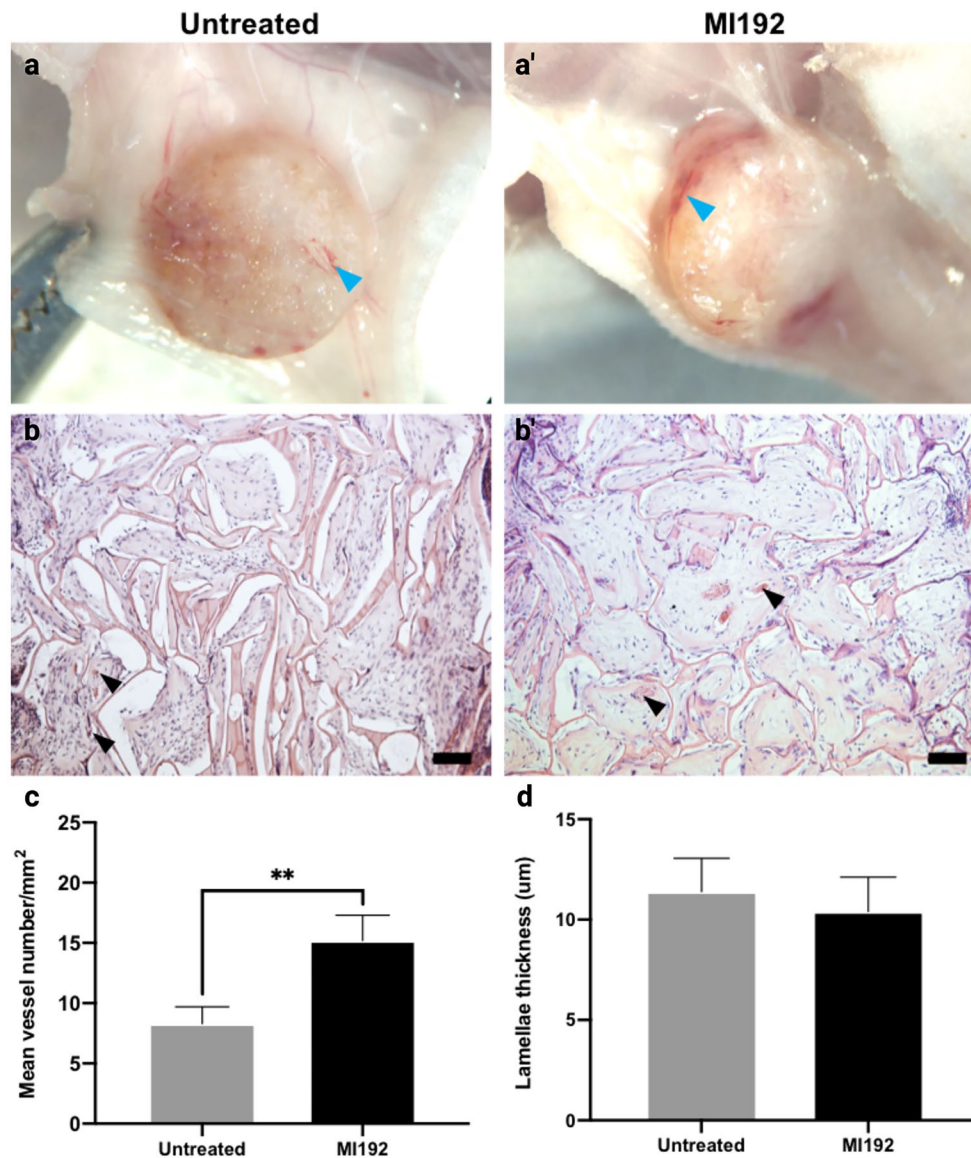
Fig. 8 Macroscopic and histological analysis for angiogenesis and scaffold degradation of MI192 pre-treated hDPSCs-silk constructs following 6 weeks subcutaneous implantation in mice. **a** and **a'** Macroscopic image of cell-laden construct immediately prior to extraction. Light blue arrowheads highlight blood vessel formation. **b** and **b'** H&E staining showing hDPSCs throughout the silk constructs with subcutaneous tissues at the periphery. Black arrowheads highlight blood vessel infiltration. Scale bars = 100 μm. **c** Blood vessel density in hDPSC-silk scaffolds quantified from histological images. **d** Internal lamellae thickness. Data represented as mean ± SD ($n = 3$). ** $P \leq 0.01$

shape significantly enhanced osteoblast mineralisation via hyperacetylation-induced gene activation when compared to cells on 3D-printed constructs exhibiting a square pore conformation (Man et al. 2021d). Altogether, these findings indicate the importance of silk concentration in modulating the key physical properties of the scaffolds, ultimately impacting its potential clinical utility for bone augmentation strategies.

The behaviour of MSCs is tightly regulated by the microenvironments in which they reside, where the external factors affect the key cellular processes such as proliferation and differentiation (Breuls et al. 2008; Maioli et al. 2018). ALP activity, an early marker of osteogenesis, was assessed to initially determine the influence of the silk scaffold concentration on hDPSCs osteogenesis with/without MI192 pretreatment. In both scaffold types, MI192 pre-treated hDPSCs exhibited a significantly elevated ALPSA compared to the untreated cells, consistent with the treatment with MI192-enhanced hDPSCs ALPSA observed in 2D in vitro (Man et al. 2021b). Interestingly, the MI192-induced increase in
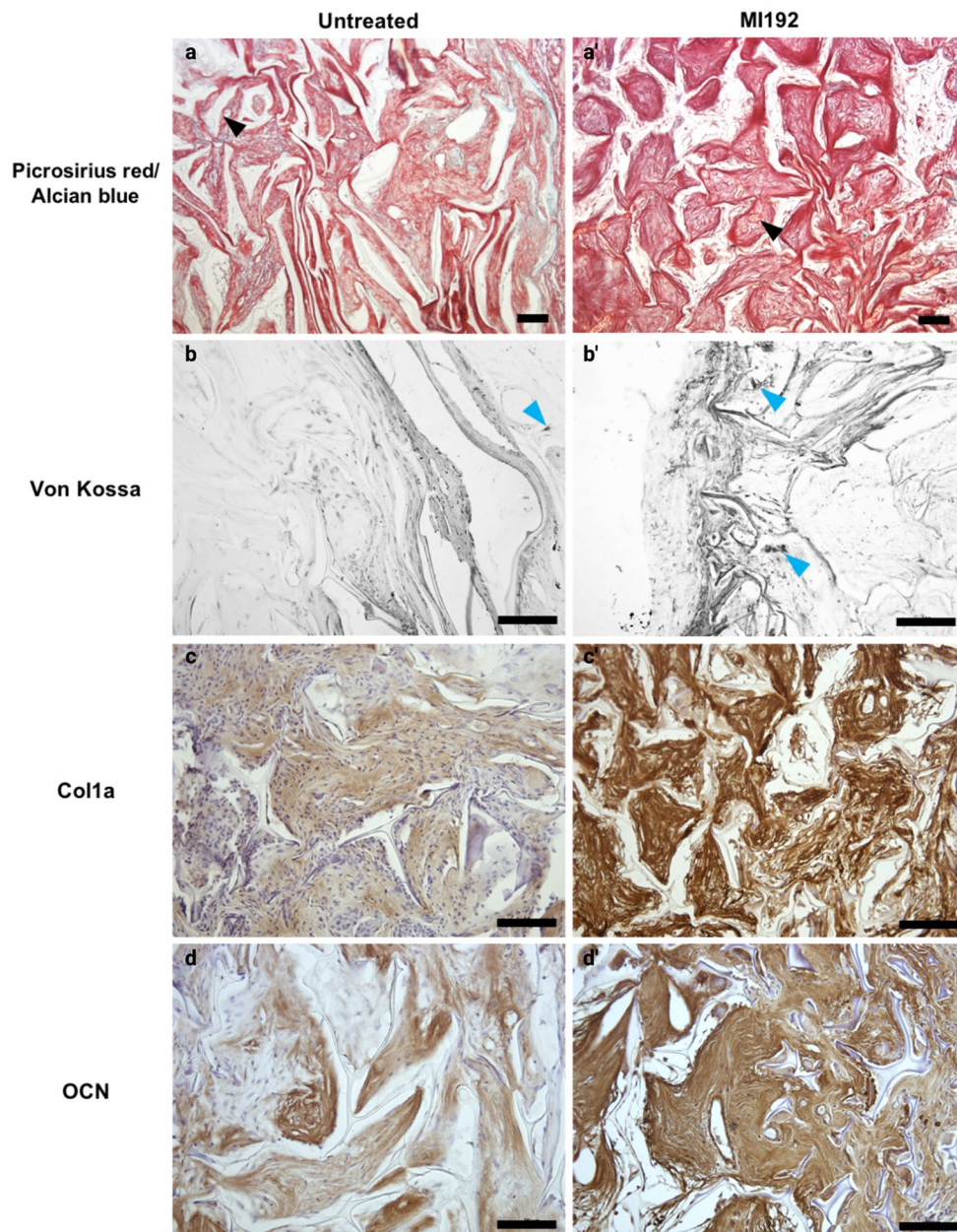
Fig. 9 Histological and immunohistochemical staining of extracellular bone matrix and mineralisation of MI192 pre-treated hDPSCs within silk constructs following 6 weeks subcutaneous implantation in mice. Positive histological staining for collagen (red colour, picrosirius red/alcian blue staining) and black arrowheads indicated vessel formation (**a**, **a'**). Mineral nodule formation (black colour — light blue arrows, Von Kossa staining) (**b**, **b'**). Production of type I collagen (**c**, **c'**) and OCN (**d**, **d'**) proteins was evaluated via immunohistochemical staining (brown colour). Scale bar, 100 µm

hDPSCs ALPSA was slightly more remarkable in the silk scaffolds (~2 folds) when compared to that in 2D culture (1.68 fold), likely due to the influence of the scaffold 3D microenvironment on promoting osteogenesis (Ghasemi-Mobarakeh et al. 2015; Sun et al. 2018). These findings demonstrate that MI192 is capable of promoting hDPSCs osteogenic differentiation within this 3D culture model, correlating with the enhanced ALPSA of MI192-treated hBMSCs when cultured as bio-assembled microtissues (BMT) (Man et al. 2021c). Moreover, our findings also showed that ALPSA of both MI192 pre-treated and untreated cells were significantly increased in the 5 wt% silk scaffolds compared to their respective cells in the 2 wt% silk scaffolds (1.27 and 1.44 fold, respectively). These results imply that the increased stiffness exerted by increasing the polymer concentration plays an important role in modulating the osteogenic

capacity of hDPSCs (Engler et al. 2006; Witkowska-Zimny et al. 2013). These findings also indicate the importance of silk concentration not only for supporting the bone defect site mechanics but also in stimulating MSCs differentiation (Ghasemi-Mobarakeh et al. 2015; Sun et al. 2018). Therefore, the 5 wt% construct was utilised to further assess the effects of MI192 on promoting hDPSCs osteogenic differentiation within the silk scaffolds.

Several studies have reported enhanced transcriptional activity and gene activation induced by HDACis (Jin et al. 2013; Schroeder et al. 2004). Although the efficacy of MI192 to stimulate hDPSCs osteoblast-related gene expression has been shown in 2D culture (Man et al. 2021b), it is important to evaluate its ability to promote osteogenesis within a more physiologically relevant environment. Our findings showed that MI192 accelerated the expression profiles of the early osteogenic genes *Runx2* and *ALP* within hDPSCs compared to the untreated control. Moreover, the expressions of the mid-late stage osteogenic genes *Col1a* and *OCN* were also significantly upregulated in MI192 pre-treated cells within the silk scaffolds during osteoinductive culture. These findings show the capability of MI192 in enhancing the expression of osteoblast-related markers, which are integral in promoting hDPSCs lineage-specific differentiation (Jonason et al. 2009; Sasano et al. 1993). The increased osteoblast-related gene expression observed in this study is consistent with the findings from MI192 pre-treated hDPSCs in 2D culture (Man et al. 2021a) and MI192 pre-treated hBMSCs in the BMT model (Man et al. 2021c). Collectively, these results suggest the plasticity of MI192 in promoting the osteogenesis of MSCs derived from different tissues and cultured in various model systems. It is important to note that MI192-enhanced hDPSCs osteogenesis is likely due to the increased chromatin's transcriptional permissiveness similar to panHDACis mechanism. However, due to its selective inhibition of HDAC3, such effects may result in enhancing the transcriptional activity and stability of Runx2 (Jonason et al. 2009). Therefore, it is probable that the MI192 pre-treated cells exhibited increased transcriptionally active Runx2, although further investigation is required.

Histological analysis was conducted to evaluate the effects of MI192 on stimulating hDPSCs extracellular matrix deposition within the silk scaffolds. The MI192 pre-treated group exhibited substantially increased collagen deposition confirmed via picrosirius red staining when compared to the untreated control, similar to the work performed previously with MI192 pre-treated ADSCs on *Antheraea mylitta* (AM) silk scaffolds (Lawlor 2016). Further evaluation by immunohistochemical analysis showed that both untreated and MI192 pre-treated constructs exhibited positive expression of osteoblast-related proteins ALP, Col1a and OCN. Interestingly, the MI192 pre-treated constructs displayed substantially increased expression for all these assessed osteogenic

markers compared to the untreated group, consistent with the upregulated osteogenic gene expression and ALPSA findings in this study. Similarly, it was also reported that MI192 promoted the osteoblast-related protein expression of hBMSCs when cultured in the BMT model (Man et al. 2021c). Paino et al. (2014) demonstrated that valproic acid (VPA) pre-treatment promoted hDPSCs collagen deposition whilst inhibiting OCN protein expression in lyophilised collagen type I scaffolds (Paino et al. 2014), indicating the effect of VPA in inhibiting terminal differentiation of hDPSCs. Intriguingly, this was not observed in our study, likely due to the increased HDAC isoform selectivity of MI192 towards HDAC3 compared to VPA. Previously, it was shown that MI192 enhanced ADSCs expression of Col1a but not OCN in Antheraea mylitta (AM) silk scaffolds (Lawlor 2016), which differed from the findings in this study. Probably, the higher wt% scaffolds and the different MSCs type utilised in this study resulted in the elevated expression of OCN. The enhanced deposition of osteoblast-related extracellular matrix proteins following osteogenic culture is likely facilitated by the slow-on/off binding kinetics of MI192 to HDAC isoforms when compared to other HDACis as reported by Boissinot et al. (Boissinot et al. 2012). Therefore, the slow-binding kinetics of MI192 possibly potentiates the augmented epigenetic function within the pre-treated hDPSCs in silk scaffolds during osteogenic culture, similar to the findings observed in 2D culture (Man et al. 2021b). Thus, these findings demonstrate that MI192 pre-treatment is able to stimulate hDPSCs deposition of osteoblast-related extracellular matrix proteins within silk scaffolds in vitro.

The effects of MI192 on hDPSCs calcium deposition and mineralisation were assessed via alizarin red and Von Kossa staining, respectively. Both groups displayed positive calcium deposition within the scaffolds. However, the MI192 pre-treated cells exhibited significantly increased calcium content (1.78 fold) compared to untreated cells. A similar profile was observed following Von Kossa staining, and the MI192 pre-treated group displayed substantially enhanced mineral nodule formation. These findings correlate well with the enhanced mineralisation observed with the MI192 pre-treated ADSCs in the AM silk scaffolds (Lawlor 2016) and VPA pre-treated hDPSCs in the Gingistat scaffolds (Paino et al. 2014). The areas with the most significant calcium and mineral deposition in the scaffolds corresponded to the regions of increased extracellular protein expression, indicating cells of a more mature osteogenic phenotype in these locations. A number of studies showed that the extracellular matrix proteins sequester bioactive factors in the cells' secretome involved in mineral nucleation (Blaser and Aikawa 2018; Man et al. 2020). Interestingly, extracellular vesicles (EVs) derived from epigenetically-modified osteoblasts were shown to significantly increase MSCs matrix mineralisation when compared to EVs from unmodified cells

(Man et al. 2021a). Hence, it is likely the secretome plays a critical role in promoting extracellular matrix mineralisation of MI192 pre-treated hDPSCs within the scaffolds.

There have been limited reports investigating the efficacy of HDACis to promote MSCs osteogenic differentiation in vivo (Huynh et al. 2017; Jung et al. 2010; Lee et al. 2011), and the majority of these studies have harnessed panHDACis, which are associated with several issues (Lawlor 2016; Yang et al. 2017). In the present study, the effects of MI192 on stimulating hDPSCs bone-like tissue formation within the silk scaffolds were assessed in vivo via subcutaneous implantation. Vascularisation of scaffolds targeted for critical-sized defects is an essential requirement for developing functional bone constructs, as the lack of necessary nutrient/waste exchange may lead to necrosis within the scaffold and ultimately result in inadequate integration into the host tissues (Rouwkema et al. 2008). Vascular ingrowth from the surrounding subcutaneous tissues was observed via histological analysis in both groups, indicating the silk scaffold provides a favourable microenvironment for vascularisation, which has been similarly shown in the literature (Han et al. 2016; Lin et al. 2020). Interestingly, we reported a significant increase in the blood vessel density within the MI192 pre-treated cells in the silk scaffolds compared to the untreated cells. This may indicate the role of HDACi treatment on augmenting the secreted trophic factors, such as cytokines or EVs from the hDPSCs in vivo, resulting in enhanced recruitment of endothelial cells into the scaffolds (Diomede et al. 2018; Man et al. 2020), although this would require further investigation. Park and co-workers (2010) reported that the silk scaffold degradation rate is linked to improved bone-like tissue formation (Park et al. 2010). Histological analysis showed a reduced scaffold volume in the MI192 pre-treated constructs compared to the untreated control, indicating enhanced de novo tissue formation within the scaffolds.

Moreover, faster scaffold degradation rates have been suggested to facilitate vascular infiltration and vessel formation (Zhang et al. 2019), consistent with our vascularisation findings. The MI192 pre-treated groups exhibited increased extracellular matrix deposition observed through picrosirius red collagen staining and immunostaining of Col1a and OCN, similar to our in vitro data, providing further evidence supporting the efficacy of this HDACi in promoting hDPSCs osteogenic capacity. Importantly, the MI192 pre-treated constructs exhibited an increased quantity of mineral nodules. The enhanced extracellular matrix deposition and mineral formation observed from the MI192 pre-treated hDPSCs were consistent with the elevated collagen production and mineral deposition observed from MI192 pre-treated ADSCs within AM silk scaffolds in vitro (Lawlor 2016). Similar results were found in the MI192 pre-treated hBMSCs in the BMT model in vitro and in vivo (Man et al. 2021c). These observations indicate that MI192 is capable of promoting the osteogenic lineage-specific differentiation of MSCs derived from different stem sources and cultured in different scaffold systems in vitro and in vivo. Taken together, these findings demonstrate lyophilised silk scaffolds provide a suitable platform to facilitate the delivery of MI192 pre-treated hDPSCs in vivo, enhancing its efficacy to stimulate de novo bone formation.

Looking forward, it is necessary to investigate the capacity of MI192 pre-treated hDPSCs within silk scaffolds to stimulate critical-sized bone defect repair, which would provide greater pre-clinical evidence into the translation of this cell-based approach for effective functional bone regeneration in the clinical setting.

Conclusion

In conclusion, this study provides evidence that the selective HDAC2 and 3 inhibitor MI192 is capable of promoting hDPSCs osteogenic differentiation within lyophilised *Bombyx Mori* silk scaffolds in vitro and in vivo, indicating the potential of combining epigenetic reprogramming with porous silk scaffold for enhancing the efficacy of MSCs-based therapies for bone augmentation strategies.

Declarations

References

Abbott A (2003) Cell culture: biology's new dimension. Nature 424:870–872

Allmeling C, Jokuszies A, Reimers K, Kall S, Choi CY, Brandes G, Kasper C, Scheper T, Guggenheim M, Vogt PM (2008) Spider silk fibres in artificial nerve constructs promote peripheral nerve regeneration. Cell Proliferat 41:408–420

Amini AR, Laurencin CT, Nukavarapu SP (2012) Bone tissue engineering: recent advances and challenges. Crit Rev Biomed Eng 40:363–408

Baker BM, Chen CS (2012) Deconstructing the third dimension - how 3D culture microenvironments alter cellular cues. J Cell Sci 125:3015–3024

Balasubramanian S, Verner E, Buggy JJ (2009) Isoform-specific histone deacetylase inhibitors: the next step? Cancer Lett 280:211–221

Baroli B (2009) From natural bone grafts to tissue engineering therapeutics: brainstorming on pharmaceutical formulative requirements and challenges. J Pharm Sci-Us 98:1317–1375

Barroso IA, Man K, Villapun VM, Cox SC, Ghag AK (2021) Methacrylated silk fibroin hydrogels: pH as a tool to control functionality. ACS Biomater Sci Eng 7:4779–4791

Berthiaume F, Maguire TJ, Yarmush ML (2011) Tissue engineering and regenerative medicine: history, progress, and challenges. Annu Rev Chem Biomol 2:403–430

Blaser MC, Aikawa E (2018) Roles and regulation of extracellular vesicles in cardiovascular mineral metabolism. Front Cardiovasc Med 5:187

Boissinot M, Inman M, Hempshall A, James SR, Gill JH, Selby P, Bowen DT, Grigg R, Cockerill PN (2012) Induction of differentiation and apoptosis in leukaemic cell lines by the novel benzamide family histone deacetylase 2 and 3 inhibitor MI-192. Leukemia Res 36:1304–1310

Breuls RG, Jiya TU, Smit TH (2008) Scaffold stiffness influences cell behavior: opportunities for skeletal tissue engineering. Open J Orthop 2:103–109

Chance-Larsen K, Backhouse MR, Collier R, Wright C, Gosling S, Harden B, Marsh S, Kay P, Wyles H, Erwin J, Woolf A (2019) Developing a national musculoskeletal core capabilities framework for first point of contact practitioners. Rheumatol Adv Pract 3:Artn: rkz036

Cho HH, Park HT, Kim YJ, Bae YC, Suh KT, Jung JS (2005) Induction of osteogenic differentiation of human mesenchymal stem cells by histone deacetylase inhibitors. J Cell Biochem 96:533–542

Correia C, Bhumiratana S, Yan LP, Oliveira AL, Gimble JM, Rockwood D, Kaplan DL, Sousa RA, Reis RL, Vunjak-Novakovic G (2012) Development of silk-based scaffolds for tissue engineering of bone from human adipose-derived stem cells. Acta Biomater 8:2483–2492

de Boer J, Licht R, Bongers M, van der Klundert T, Arends R, van Blitterswijk C (2006) Inhibition of histone acetylation as a tool in bone tissue engineering. Tissue Eng 12:2927–2937

Dimitriou R, Jones E, McGonagle D, Giannoudis PV (2011) Bone regeneration: current concepts and future directions. Bmc Med 9:Artn 66

Diomede F, Gugliandolo A, Scionti D, Merciaro I, Cavalcanti MF, Mazzon E, Trubiani O (2018) Biotherapeutic effect of gingival stem cells conditioned medium in bone tissue restoration. Int J Mol Sci 19:329

Downing TL, Soto J, Morez C, Houssin T, Fritz A, Yuan FL, Chu JL, Patel S, Schaffer DV, Li S (2013) Biophysical regulation of epigenetic state and cell reprogramming. Nat Mater 12:1154–1162

El-Gendy R, Yang XB, Newby PJ, Boccaccini AR, Kirkham J (2013) Osteogenic differentiation of human dental pulp stromal cells on 45S5 bioglass (R) based scaffolds in vitro and in vivo. Tissue Eng Pt A 19:707–715

Engler AJ, Sen S, Sweeney HL, Discher DE (2006) Matrix elasticity directs stem cell lineage specification. Cell 126:677–689

Genetics Home Reference (2021) Is gene therapy safe? , vol 2021. National Library of Medicine, MedlinePlus, pp https://medlineplus.gov/genetics/understanding/therapy/safety/

Ghasemi-Mobarakeh L, Prabhakaran MP, Tian LL, Shamirzaei-Jeshvaghani E, Dehghani L, Ramakrishna S (2015) Structural properties of scaffolds: crucial parameters towards stem cells differentiation. World J Stem Cells 7:728–744

Gryder BE, Sodji QH, Oyelere AK (2012) Targeted cancer therapy: giving histone deacetylase inhibitors all they need to succeed. Future Med Chem 4:505–524

Han H, Ning H, Liu S, Lu QP, Fan Z, Lu H, Lu G, Kaplan DL (2016) Silk biomaterials with vascularization capacity. Adv Func Mater 26:421–436

Han QQ, Yang PS, Wu YW, Meng S, Sui L, Zhang L, Yu LM, Tang Y, Jiang H, Xuan DY, Kaplan DL, Kim SH, Tu QS, Chen J (2015) Epigenetically modified bone marrow stromal cells in silk scaffolds promote craniofacial bone repair and wound healing. Tissue Eng Pt A 21:2156–2165

Hu XQ, Zhang X, Dai LH, Zhu JX, Jia ZQ, Wang WP, Zhou CY, Ao YF (2013) Histone deacetylase inhibitor trichostatin A promotes the osteogenic differentiation of rat adipose-derived stem cells by altering the epigenetic modifications on Runx2 promoter in a BMP signaling-dependent manner. Stem Cells Dev 22:248–255

Huynh NC, Everts V, Pavasant P, Ampornaramveth RS (2016) Inhibition of histone deacetylases enhances the osteogenic differentiation of human periodontal ligament cells. J Cell Biochem 117:1384–1395

Huynh NCN, Everts V, Nifuji A, Pavasant P, Ampornaramveth RS (2017) Histone deacetylase inhibition enhances in-vivo bone regeneration induced by human periodontal ligament cells. Bone 95:76–84

Jin H, Park JY, Choi H, Choung PH (2013) HDAC inhibitor trichostatin A promotes proliferation and odontoblast differentiation of human dental pulp stem cells. Tissue Eng Pt A 19:613–624

Jonason JH, Xiao G, Zhang M, Xing L, Chen D (2009) Post-translational regulation of Runx2 in bone and cartilage. J Dent Res 88:693–703

Joukhdar H, Seifert A, Jungst T, Groll J, Lord MS, Rnjak-Kovacina J (2021) Ice templating soft matter: fundamental principles and fabrication approaches to tailor pore structure and morphology and their biomedical applications. Adv Mater 33:ARTN: 2100091

Jung HM, Song GA, Lee YK, Baek JH, Ryoo HM, Kim GS, Choung PH, Woo KM (2010) Modulation of the resorption and osteoconductivity of alpha-calcium sulfate by histone deacetylase inhibitors. Biomaterials 31:29–37

Lawlor L (2016) The Effect of HDAC Inhibitor MI192 on stem cell behaviour-the potential of utilising MI192 for bone tissue engineering. Department of Oral Biology and EPSRC Doctoral Training Centre for Tissue Engineering and Regenerative Medicine., vol PhD. University of Leeds, https://etheses.whiterose.ac.uk/13512/, pp 313

Lawlor L, Yang XB (2019) Harnessing the HDAC-histone deacetylase enzymes, inhibitors and how these can be utilised in tissue engineering. Int J Oral Sci 11:ARTN: 20

Lee SU, Kwak HB, Pi SH, You HK, Byeon SR, Ying Y, Luesch H, Hong J, Kim SH (2011) In vitro and in vivo osteogenic activity of largazole. ACS Med Chem Lett 2:248–251

Li Y, Chu JS, Kurpinski K, Li X, Bautista DM, Yang L, Sung KLP, Li S (2011) Biophysical regulation of histone acetylation in mesenchymal stem cells. Biophys J 100:1902–1909

Lin X, Tang F, Jiang S, Khamis H, Bongers A, Whitelock JM, Lord MS, Rnjak-Kovacina J (2020) A biomimetic approach toward enhancing angiogenesis: recombinantly expressed domain V of human perlecan is a bioactive molecule that promotes angiogenesis and vascularization of implanted biomaterials. Adv Sci (weinh) 7:2000900

Maioli M, Redl H, Stoddart MJ (2018) Environmental influences on stem cell behavior. Stem Cells Int 2018:Artn: 7415460

Man K, Brunet MY, Jones MC, Cox SC (2020) Engineered extracellular vesicles: tailored-made nanomaterials for medical applications. Nanomaterials-Basel 10:ARTN: 1838

Man K, Brunet MY, Fernandez-Rhodes M, Williams S, Heaney LM, Gethings LA, Federici A, Davies OG, Hoey D, Cox SC (2021a) Epigenetic reprogramming enhances the therapeutic efficacy of osteoblast-derived extracellular vesicles to promote human bone marrow stem cell osteogenic differentiation. Journal of Extracellular Vesicles 10:e12118

Man K, Lawlor L, Jiang L-H, Yang XB (2021b) The selective histone deacetylase inhibitor MI192 enhances the osteogenic differentiation efficacy of human dental pulp stromal cells. Int J Mol Sci 22:1–17

Man K, Mekhileri N, Lim K, Jiang LH, Woodfield T, Yang XB (2021c) MI192 induced epigenetic reprogramming enhances the therapeutic efficacy of human bone marrows stromal cells for bone regeneration. Bone 153:116138

Man K, Brunet MY, Louth S, Robinson TE, Fernandez-Rhodes M, Williams S, Federici AS, Davies OG, Hoey DA, Cox SC (2021d) Development of a bone-mimetic 3D printed Ti6Al4V scaffold to enhance osteoblast-derived extracellular vesicles' therapeutic efficacy for bone regeneration. Frontiers in Bioengineering and Biotechnology 9:757290

Marks PA (2010) Histone deacetylase inhibitors: a chemical genetics approach to understanding cellular functions. Bba-Gene Regul Mech 1799:717–725

Maroni P, Brini AT, Arrigoni E, de Girolamo L, Niada S, Matteucci E, Bendinelli P, Desiderio MA (2012) Chemical and genetic blockade of HDACs enhances osteogenic differentiation of human adipose tissue-derived stem cells by oppositely affecting osteogenic and adipogenic transcription factors. Biochem Biophys Res Commun 428:271–277

Meinel L, Fajardo R, Hofmann S, Langer R, Chen J, Snyder B, Vunjak-Novakovic G, Kaplan D (2005) Silk implants for the healing of critical size bone defects. Bone 37:688–698

Melke J, Midha S, Ghosh S, Ito K, Hofmann S (2016) Silk fibroin as biomaterial for bone tissue engineering. Acta Biomater 31:1–16

Paino F, La Noce M, Tirino V, Naddeo P, Desiderio V, Pirozzi G, De Rosa A, Laino L, Altucci L, Papaccio G (2014) Histone deacetylase inhibition with valproic acid downregulates osteocalcin gene expression in human dental pulp stem cells and osteoblasts: evidence for HDAC2 involvement. Stem Cells 32:279–289

Park SH, Gil ES, Shi H, Kim HJ, Lee K, Kaplan DL (2010) Relationships between degradability of silk scaffolds and osteogenesis. Biomaterials 31:6162–6172

Patra C, Talukdar S, Novoyatleva T, Velagala SR, Muhlfeld C, Kundu B, Kundu SC, Engel FB (2012) Silk protein fibroin from Antheraea mylitta for cardiac tissue engineering. Biomaterials 33:2673–2680

Rnjak-Kovacina J, Wray LS, Burke KA, Torregrosa T, Golinski JM, Huang W, Kaplan DL (2015) Lyophilized silk sponges: a versatile biomaterial platform for soft tissue engineering. ACS Biomater Sci Eng 1:260–270

Rockwood DN, Preda RC, Yucel T, Wang XQ, Lovett ML, Kaplan DL (2011) Materials fabrication from Bombyx mori silk fibroin. Nat Protoc 6:1612–1631

Rouwkema J, Rivron NC, van Blitterswijk CA (2008) Vascularization in tissue engineering. Trends Biotechnol 26:434–441

Saha S, Kundu B, Kirkham J, Wood D, Kundu SC, Yang XB (2013) Osteochondral tissue engineering in vivo: a comparative study using layered silk fibroin scaffolds from mulberry and nonmulberry silkworms. Plos One 8:ARTN: e80004

Sasano Y, Ohtani E, Narita K, Kagayama M, Murata M, Saito T, Shigenobu K, Takita H, Mizuno M, Kuboki Y (1993) Bmps induce direct bone-formation in ectopic sites independent of the endochondral ossification invivo. Anat Rec 236:373–380

Schroeder TM, Kahler RA, Li XD, Westendorf JJ (2004) Histone deacetylase 3 interacts with Runx2 to repress the osteocalcin promoter and regulate osteoblast differentiation. J Biol Chem 279:41998–42007

Schroeder TM, Westendorf JJ (2005) Histone deacetylase inhibitors promote osteoblast maturation. J Bone Miner Res 20:2254–2263

Sun M, Chi G, Xu J, Tan Y, Xu J, Lv S, Xu Z, Xia Y, Li L, Li Y (2018) Extracellular matrix stiffness controls osteogenic differentiation of mesenchymal stem cells mediated by integrin alpha5. Stem Cell Res Ther 9:52

Sun WZ, Gregory DA, Tomeh MA, Zhao XB (2021) Silk fibroin as a functional biomaterial for tissue engineering. Int J Mol Sci 22:ARTN: 1499

Tollervey JR, Lunyak VV (2012) Epigenetics Judge, jury and executioner of stem cell fate. Epigenetics-Us 7:823–840

Uebersax L, Hagenmuller H, Hofmann S, Gruenblatt E, Muller R, Vunjak-Novakovic G, Kaplan DL, Merkle HP, Meinel L (2006) Effect of scaffold design on bone morphology in vitro. Tissue Eng 12:3417–3429

Varkey A, Venugopal E, Sugumaran P, Janarthanan G, Pillai MM, Rajendran S, Bhattacharyya A (2015) Impact of silk fibroin-based scaffold structures on human osteoblast MG63 cell attachment and proliferation. Int J Nanomedicine 10(Suppl 1):43–51

von Byern J, Chandler P, Merritt D, Adlassnig W, Stringer I, Meyer-Rochow VB, Kovalev A, Dorrer V, Dimartino S, Marchetti-Deschmann M, Gorb S (2019) Biomechanical properties of fishing lines of the glowworm Arachnocampa luminosa (Diptera; Keroplatidae). Sci Rep-Uk 9:ARTN: 3082

Witkowska-Zimny M, Walenko K, Wrobel E, Mrowka P, Mikulska A, Przybylski J (2013) Effect of substrate stiffness on the osteogenic differentiation of bone marrow stem cells and bone-derived cells. Cell Biol Int 37:608–616

Xu WS, Parmigiani RB, Marks PA (2007) Histone deacetylase inhibitors: molecular mechanisms of action. Oncogene 26:5541–5552

Yamauchi Y, Cooper PR, Shimizu E, Kobayashi Y, Smith AJ, Duncan HF (2020) Histone acetylation as a regenerative target in the dentine-pulp complex. Front Genet 11:1

Yang SS, Zhang R, Wang G, Zhang YF (2017) The development prospection of HDAC inhibitors as a potential therapeutic direction in Alzheimer's disease. Transl Neurodegener 6:ARTN: 19

Yang XJ, Seto E (2007) HATs and HDACs: from structure, function and regulation to novel strategies for therapy and prevention. Oncogene 26:5310–5318

Yoshioka T, Tsubota T, Tashiro K, Jouraku A, Kameda T (2019) A study of the extraordinarily strong and tough silk produced by bagworms. Nat Commun 10:ARTN: 1469

Zhang L, Liu X, Li G, Wang P, Yang Y (2019) Tailoring degradation rates of silk fibroin scaffolds for tissue engineering. J Biomed Mater Res A 107:104–113

Zhao J, Zhang ZY, Wang SY, Sun XJ, Zhang XL, Chen J, Kaplan DL, Jiang XQ (2009) Apatite-coated silk fibroin scaffolds to healing mandibular border defects in canines. Bone 45:517–527